Solid Freeform Fabrication 2016: Proceedings of the 27th Annual International Solid Freeform Fabrication Symposium – An Additive Manufacturing Conference
Reviewed Paper

Planning the process parameters during Direct Metal Deposition of functionally graded thin-walled parts based on a 2D model

Jingyuan Yan[1], Ilenia Battiato[2], and Georges M. Fadel[1]

[1]Department of Mechanical Engineering, Clemson University, Clemson, SC 29634
[2]Department of Mechanical Engineering, San Diego State University, San Diego, CA 92182

Abstract

The need for functionally graded material (FGM) parts has surfaced with the development of material science and additive manufacturing techniques. Direct Metal Deposition (DMD) processes can locally deposit different metallic powders to produce FGM parts. Yet inappropriate mixing of materials without considering the influence of varying dilution rates and the variation of material properties can result in inaccurate material composition ratios when compared to the desired or computed compositions. Within such a context, this paper proposes a 2D simulation based design method for planning the process parameters in the DMD manufacturing of designed thin-walled parts. The proposed scheme is illustrated through two case studies, one of which is a part with one-dimensional varying composition and the other with two dimensional variation. Using the proposed method, the process parameters can be planned prior to the manufacturing process, and the material distribution deviation from the desired one can be reduced.

1. Introduction

Additive manufacturing of metals is becoming of strategic importance in a variety of industries. Direct Metal Deposition (DMD) stands out among metal based additive manufacturing techniques due to its flexibility in depositing powders. Because of this, the potential of the DMD process greatly lies on the fabrication of heterogeneous objects.

A heterogeneous object is non-uniform, and composed of different materials (or phases) with different properties. A heterogeneous object has many advantages and can realize appearance and/or functionality that homogeneous objects cannot achieve, such as the enhancement of the overall physical properties of the object, or cost and weight reduction. Based on the material distribution, heterogeneous objects can also be classified into two categories: HCs (Heterogeneous Continuous) and HDs (Heterogeneous Discrete) [1, 2]. HCs have a continuous material distribution function while HDs have a discrete material distribution function. The HCs are also named functionally graded materials (FGM). Although fabricating HCs or FGM parts is our final goal, when coming to the manufacturing process, discretization is a realistic and practical approach. The process parameters are tuned according to the design requirements in a discrete or step-by-step manner due to the nature of the digital control of the machines. The manufacturing resolution depends on parameters such as the control step size, the powder size, the laser scanning speed, and the laser beam dimension.

Among the currently existing metal based additive manufacturing techniques, such as Direct Metal Deposition (DMD), Ultrasonic Consolidation (UC), Shape Deposition Manufacturing (SDM), Selective Laser Melting (SLM), and Electron Beam Melting (EBM), DMD has the added flexibility of being able to vary the proportion of different materials spatially and

continuously. Most of the other processes typically can only vary materials in a layer by layer fashion. The DMD process can deliver powders either via powders premixing [3-8], or via powders in-situ mixing [9-12]. In this study, the focus is the fabrication of heterogeneous objects using the in-situ mixing approach. The main advantage of this approach is that the powder composition can be adjusted and injected on demand.

The schematic of the DMD working space is shown in Fig. 1, where the part being fabricated is an FGM part. Two types of powders are injected and mixed in the melt pool induced by the laser beam. The final part is fabricated layer by layer, and the material composition can be varied per line and per point. The powder delivery system in this study consists of two symmetric injection nozzles. The ratio of the two powders is adjustable according to design and manufacturing requirements. The delay effect due to the length of the hose and/or nozzles is to be considered by introducing a delay.

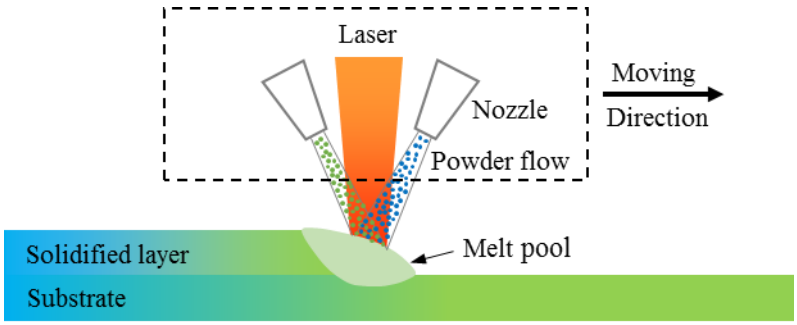

Fig. 1 Schematic of the DMD fabrication of a functionally graded part.

2. Background and Research Objective

In order to fully take advantage of the potential of heterogeneity in objects, the ability to manufacture the material distribution and shape according to a part's design is needed. Previous studies have shown that DMD and similar processes (e.g. laser cladding, laser engineered net shaping, direct laser fabrication, etc.) have the potential for fabricating FGM parts, and some of the research work has been well summarized by Qi et al. [13]. Many other publications are focused on the characterization of the FGM parts built by the DMD process. For example, Ocylok et al. used tensile tests and hardness tests to study the mechanical strength of the FGM parts made of Marlok and Stellite 31 powders [14]. Soodi et al. investigated the tensile strength and fracture mechanisms of FGM parts using different metal/alloy powders, i.e. 316 SS with 420 SS, Colmonoy6 with 316 SS, AlBrnz with 420 SS, and 316 SS with tool steel [15]. The effects of laser power and powder mass flow rates of SS316L and Inconel 718 on the microstructure and physical properties such as hardness, wear resistance, and tensile strength of FGM were discussed by Shah et al. [16]. In the majority of these publications, titanium alloys, nickel alloys, and stainless steels are the materials mostly utilized for deposition. The published results show the improvement of material properties when compared to a homogeneous material.

Ever since multi-material deposition using the LENS^{TM} technology was raised and published in the late 1990s [17], the investigation and fabrication of simple FGM parts have been implemented in a number of papers [18-26]. However, in these papers, the deposition was uniform throughout each deposition of a straight line or circular line, allowing a change only at the next deposition, which constrains the potential of the heterogeneous manufacturing capability and its

flexibility. The papers also neglect the mixed/shared portion of a certain layer with its adjacent layers, which would cause inaccuracies, especially when the resolution and/or accuracy requirements for manufacturing is high. Meanwhile, to our knowledge, the investigation of composition change point by point has not been researched or published. Without considering the varying parameters during the fabrication process, e.g., varying dilution rates and substrate properties, the final component mixing ratio will be inaccurate. Therefore, this study aims to understand, model, and propose a methodology for planning the appropriate process parameters with respect to the desired material distribution in an FGM part.

Theoretically, DMD has the potential to process and mix a vast majority of metals and alloys. Even when the laser power is not sufficiently high to fully melt one component, a discrete phase of that specific component can still form within the other component. In addition, more than two materials can be simultaneously deposited by DMD to fabricate a multi-components part according to a designed multi-material distribution. The above mentioned two conditions are beyond the scope of this work. Within this study, two typically used alloy powders (Inconel 718 and Ti-6Al-4V) are used as two build materials to investigate the basic concepts and their implementation. Since a 2D model is adopted, we only consider the scope of fabricating thin-walled heterogeneous parts.

The organization of this paper is outlined as follows. In section 3, the design methodology is proposed based on process models. Then two case studies, 1D composition change and 2D composition change respectively, are presented in section 4 to illustrate the proposed design methodology. Finally, the conclusions and future work are discussed in section 5.

3. Model Based Design Methodology

A thin-walled part can be approximated as a 2D structure where the material distribution is homogeneous in the wall thickness direction. As shown in Fig.2, the wall thickness direction is perpendicular to the paper. Basically, the volume fraction or concentration for each component material throughout the part can be analytically expressed. For manufacturing and modeling consideration, the FGM part is discretized and represented by cell arrays, as illustrated in Fig. 2. The cell volume is sufficiently small compared to the part, and the material composition remains the same within each cell. In this premise, the process parameters only vary when the laser scans across cells. According to our previous work [27, 28], many process parameters can be varied in order to achieve specific objectives such as minimize powder waste and/or laser energy consumption. These parameters include the laser power and scanning speed, the powder injection velocity and angle, and other changeable parameters. Herein we adopt a similar idea but focus on how to plan the process parameters in order to fabricate a part with specific composition variation. Since the manufacturing stability and composition control are also critical issues in this focus, some process parameters need to be preset. These parameters mainly include three categories: (1) the uniform (across the beam) attenuated value of the laser power P_{att}, laser scanning speed V, and laser spot radius r_l, since the melt pool size should be controlled; (2) the total powder volumetric feed rate $\dot{V}_p$ since the layer height should be maintained constant, the particle radius r_{pi} and particle speed v_{pi}; (3) the nozzle diameter w, and the injection angle θ_i (i = 1,2 for separate nozzles). Since varying these parameters can be computationally expensive and can even destabilize the fabrication process, the design variables only include the volumetric feed rates of the two powders $\dot{V}_{pi}$ and the actual laser power P.

The mixing of powders occurs in the melt pool, where multiple driving forces exist. The magnitude of the weld pool molten flow speed is analytically calculated about 0.5-1 m/s [29-31], and this has also been demonstrated computationally in the DMD process and the like [32-34]. With the high melt pool velocity, the mixing process can be seen as instant and uniform.

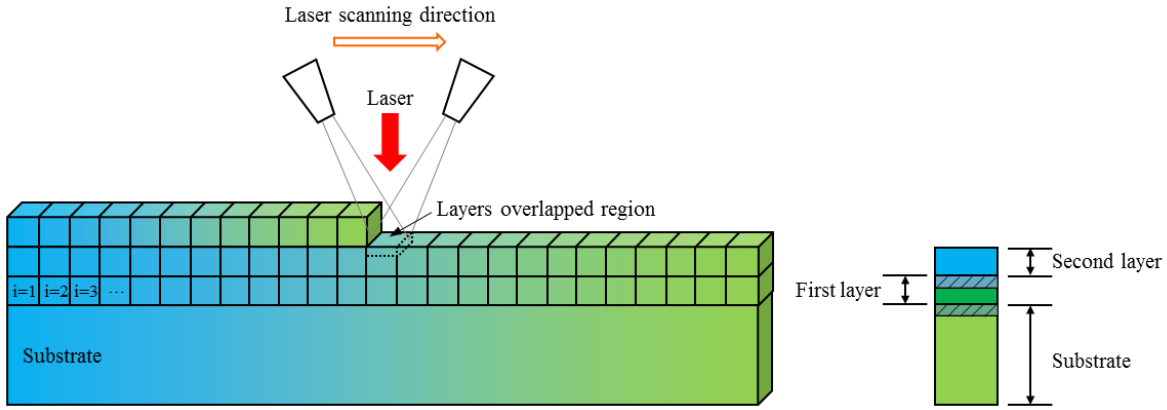

Fig. 2 Schematic illustration for part discretization and the dilution effect on mixing.

As shown in Fig. 2, the substrate based on which the FGM part is being fabricated is functionally graded. However, the substrate is typically not functionally graded but a uniform material, which is the focus in this study. The dashed cell under the laser indicates the melted region on the former layer. The shaded regions on the figure on the right (cross section) represent the shared portions between layers due to dilution. Every new layer starts on top of the previous layer, but has an overlapped region with the previous layer. The composition of a cell in the new layer is the resultant of the mixing of the instant powder composition and the composition of the cell beneath it. The dilution rate D is defined as the ratio of the cross-sectional area of the melted substrate to the total cross-sectional area of the melted substrate and the deposited layer. When determining the composition of the actual fabricated part, the effect of dilution should be considered as well as the instantaneous powder composition:

$$C_{i,des}^{1} = D_i^1 \times C_{i,sub} + (1 - D_i^1) \times C_{i,pow}^{1} \quad (2)$$

$$C_{i,des}^{2} = D_i^2 \times C_{i,des}^{1} + (1 - D_i^2) \times C_{i,pow}^{2} \quad (3)$$

$$C_{i,des}^{n} = D_i^n \times C_{i,des}^{n-1} + (1 - D_i^n) \times C_{i,pow}^{n} \quad (4)$$

where C is artificially defined as the concentration of a specific material; the superscripts represent the layer number; i is the cell number in each layer, shown in Fig. 2; the secondary subscripts indicate the layer number; and C_{des}, C_{sub}, and C_{pow} represent the desired concentration, the substrate concentration, and the powder concentration respectively. The desired concentration is a function of the dilution rate, the previous layer's concentration, and the powder concentration. Note that the concentration always refer to the same material specified.

The dilution rate can be predicted using the following equation [35].

$$D = \left(1 + \frac{\eta_d \dot{V}_p \Delta H_s}{\eta_a \eta_m P - \eta_d \dot{V}_p \Delta H_p}\right)^{-1} \tag{5}$$

where η_a, η_d and η_m are the efficiencies for laser absorption, powder deposition, and melting; $\dot{V}_p$ is the total powder volumetric feed rate (mm^3/s); P is the laser power; and ΔH_s and ΔH_p are the melting enthalpies (J/mm^3) of the substrate and the powder materials. The efficiency of laser absorption η_a includes two parts: the absorptivity due to material optical property (η_l) and the absorptivity due to the shadowing effect of powders (η_n). The melting efficiency (η_m) is defined as the fraction of the laser energy actually used for inducing the melt pool. The rest energy other than the energy used for melting is the dissipated to the unmelted region by thermal conduction. For a 2D case, the melting efficiency is given by [36, 37],

$$\eta_m = \frac{1}{\frac{8\alpha}{5Vd} + 2} \tag{6}$$

where V is the laser scanning speed; d is the melt pool width; and α is the thermal diffusivity, which is related to the material composition of the substrate. It can be seen from Eqs. (5) and (6) that the dilution rate depends on the substrate concentration, since ΔH_s, ΔH_p, and α are all functions of the substrate concentration. The substrate herein is not restricted to the original substrate, but also can be any underlying layer on top of which the new layer is being deposited.

In Eq. (5), the $\eta_a P$ term is defined as the attenuated laser power P_{att}, where $\eta_a = \eta_l \eta_n$. Considering the powder shadowing effect, η_n can be calculated using the Beer-Lambert Law [38-43], so:

$$P_{att} = \eta_l \eta_n P = \eta_l e^{-\varepsilon C_{pow} z} P \tag{7}$$

where C_{pow} is the powder concentration; $\varepsilon = \frac{3(1-\eta_l)}{2 r_p \rho_p}$ is the molar absorptivity or extinction coefficient (m^2/kg); r_p and ρ_p are the radius and density of the powder particles, and ρ_p is also dependent on the powder composition. The powder concentration is a variable along the laser scanning direction due to the overlapping of the two powder jets. However, it can be seen from Fig. 3 (a) that the two shadowed areas can be equated. Flipping the lower shadowed area, the equated shadowing effect can be represented as Fig. 3 (b), where the laser beam passes two trapezoidal regions of two materials respectively. Then, assuming the attenuation is constant within the laser beam at a specific time, Fig. 3 (b) can also be equated to Fig. 3 (c), where the laser beam passes two rectangular regions of two materials respectively. We assume that the powder injection angle is θ, the laser beam width equals to b, and neglect the powder jet divergence angle. Then Eq. (7) can be rewritten as:

$$P_{att} = \eta_l exp\left[-\frac{3(1-\eta_l)}{2 r_{p1} \rho_{p1}} \cdot \frac{\dot{V_{p1}} \rho_{p1}}{\pi \left(\frac{w}{2}\right)^2 v_{p1}} \cdot z - \frac{3(1-\eta_l)}{2 r_{p1} \rho_{p2}} \cdot \frac{\dot{V_{p2}} \rho_{p2}}{\pi \left(\frac{w}{2}\right)^2 v_{p1}} \cdot z\right] P$$

$$= \eta_l exp\left\{-\frac{6(1-\eta_l)\dot{V_{p1}}}{\pi w^2 r_{p1} v_{p1}}\left[\frac{L \sin\varphi}{sin(\theta+\varphi)} + \frac{w}{2\sin\theta}\right] - \frac{6(1-\eta_l)\dot{V_{p2}}}{\pi w^2 r_{p1} v_{p1}}\left[\frac{L \sin\varphi}{sin(\theta+\varphi)} + \frac{w}{2\sin\theta}\right]\right\} P$$

$$= \eta_l exp\left\{-\frac{6(1-\eta_l)\dot{V}_p}{\pi w^2 r_p v_p}\left[\frac{L\sin\varphi}{sin(\theta+\varphi)}+\frac{w}{2\sin\theta}\right]\right\}P \quad (for\ r_{p1}=r_{p2}\ and\ v_{p1}=v_{p2}) \tag{8}$$

Knowing the attenuated laser power, the laser power actually needed can be calculated.

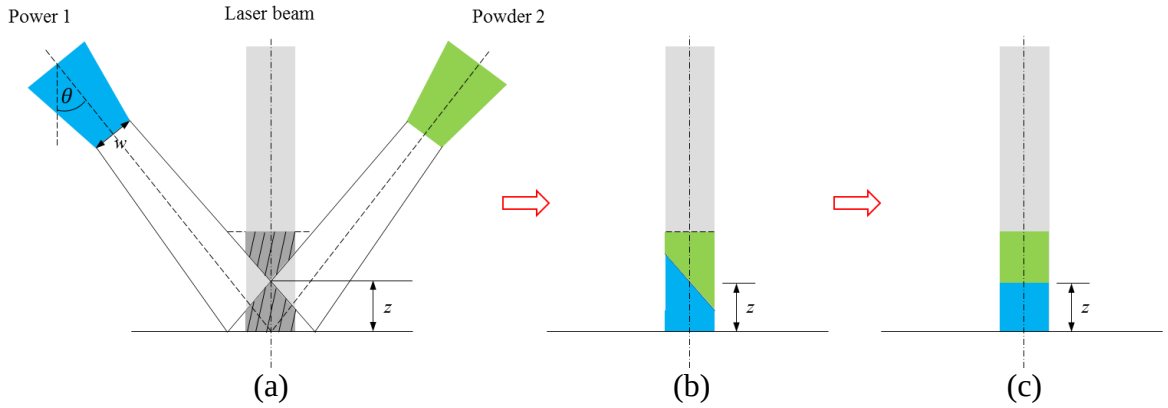

Fig. 3 Equating of the powder shadowing effect.

The attenuated laser power (P_{att}) required can be determined via FEM simulation, which will be discussed in the case studies. Then the actual laser power (P) needed can be reversely solved using Eq. (8). Based on Eq. (4), the required powder concentration ($C_{i,pow}^{n}$) at any layer and any cell can also be solved. During the calculation, the material properties of the mixture are calculated following the mixing theory:

$$P_{mixture} = (1-C)P_1 + CP_2 \tag{9}$$

where $P_{mixture}$ is any material property for the mixture, P_1 and P_2 are the material properties for material 1 and material 2 respectively. It is assumed in this study that the material properties are not variable as temperature changes. Other mixture rules could be used, our objective is to show a process, and let the engineers decide which is the most appropriate mixture rule depending on the materials they use and their own expertise. For example, the properties of the mixture can also be estimated by using the mass fractions of the two components:

$$P_{mixture} = \frac{\rho_1}{(1-C)\rho_1 + C\rho_2}(1-C)P_1 + \frac{\rho_2}{(1-C)\rho_1 + C\rho_2}CP_2 \tag{10}$$

The results of using different mixture rules are presented and compared in the case studies in Section 4. The design process that the case studies follow is illustrated in Fig. 4. The input variables are given by the designers and are circulated in the dashed rectangles, and the output variables are in the bold rectangles. Some of the input parameters have subscript i (i = 1, 2), for example, v_{pi}, r_{pi}, which represent that the specific parameter can have different values for the two types of powders.

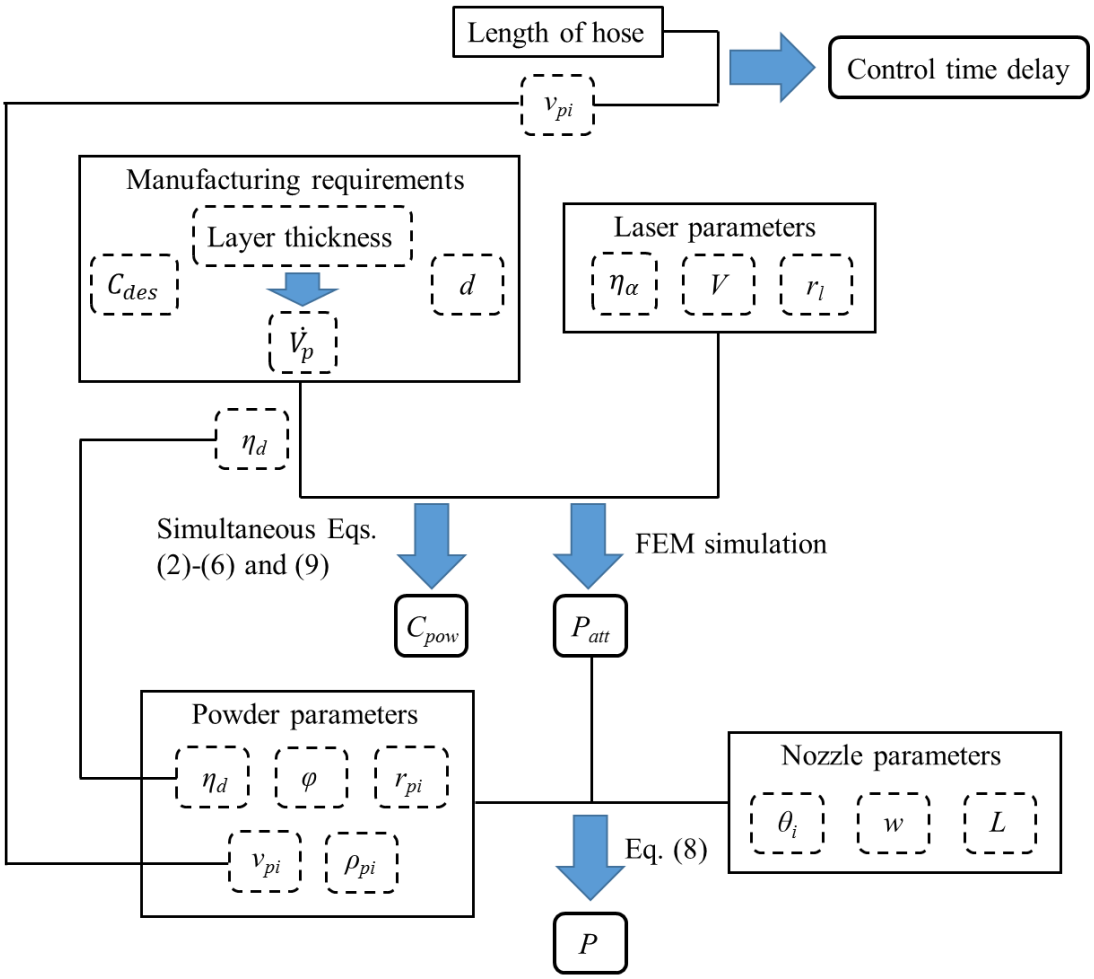

Fig. 4 Design process flowchart.

4. Case Studies

4.1 Case 1: 1D FGM Part Fabrication

The objective of this case study is to fabricate a thin-walled FGM part with dimension 3 mm × 20 mm (Fig. 5 (a)). The component materials are Inconel 718 (material 1) and Ti-6Al-4V (material 2). The physical and thermal properties of the two materials are listed in Table 1 [44-46].

The concentration in this paper is always specified for the Ti-6Al-4V. The concentration distribution of the desired part has the following function:

$$C = \frac{x}{L_x} \tag{11}$$

Consequently, the concentration for Inconel 718 is $\left(1 - \frac{x}{L_x}\right)$. For the 1D case, the concentration only varies along the *x*-axis. Therefore, the fabrication process is iterative, layer by layer, and the process parameters remain the same among layers. However, practically, the manufacturing

direction does not necessary have to follow the direction in Fig. 5 (a), the fabrication direction in Fig. 5 (b) provides a way to reduce the changing rate of powder concentration. In Fig. 5 (b), the powder concentration remains the same for every single layer. The tradeoff is that the number of layer will increase, which may affect the manufacture speed and the physical properties of the fabricated part. Determining which manufacturing direction to choose depends on different situations. In this study, we perform process parameters planning for both cases.

Table 1. Physical and thermal properties of Inconel 718 and Ti-6Al-4V.

	Inconel 718	Ti-6Al-4V
Laser absorptivity, η_l	0.3	0.3
Emissivity, E	0.4	0.4
Density, ρ (kg/m^3)	8190	4420
Specific heat, c_p (J/kg/K)	435	610
Thermal conductivity, k (W/m/K)	21.3	17.5
Thermal diffusivity, α (m^2/s)	5.98×10^{-6}	6.49×10^{-6}
Melting temperature, T_{melt} (K)	1609	1928
Melting enthalpy, ΔH (J/mm^3)	8.19	6.63

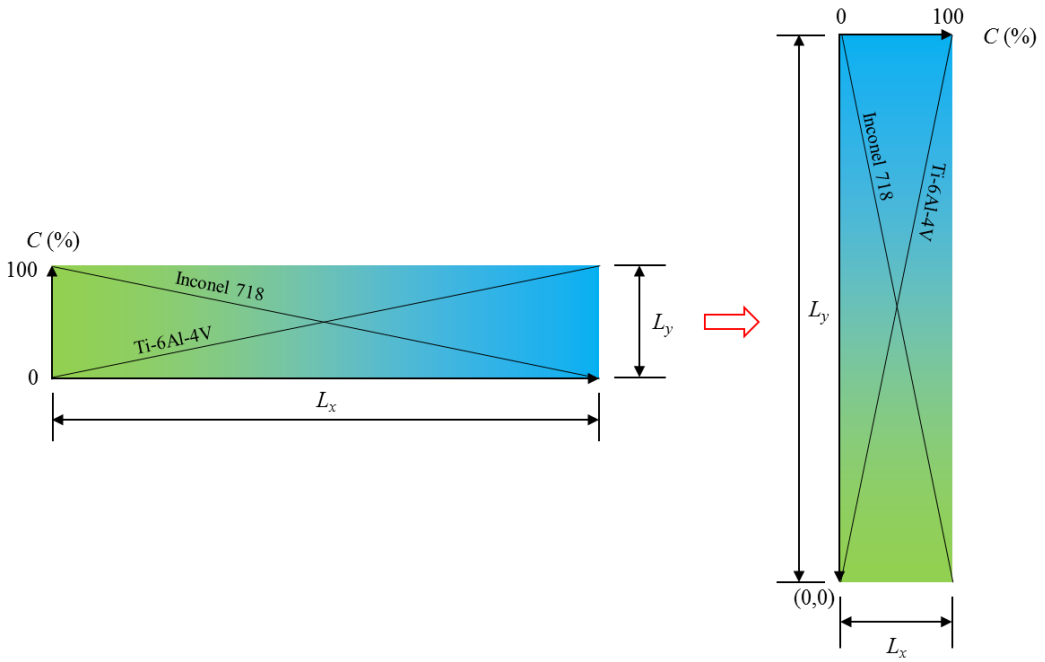

Fig. 5 FGM part with 1D concentration variation.

Case 1 (a):

Before calculating the key variables ($\dot{V}_{pl}$ and P), some constant variables need to be preset as input variables to stabilize the fabrication process. As discussed above, these preset parameters include the attenuated laser power P_{att}, laser scanning speed V, laser spot radius r_l, powder total

volumetric feed rate $\dot{V}_p$, injection angle θ_i, nozzle diameter w, particle speed v_{pi}, particle radius r_{pi}, powder divergence angle φ, the distance between the nozzle center and the spot center L, and the width (wall thickness) of the thin-walled part d. According to Eq. (8), the selection of these input parameters can affect the value of the final laser power. The laser power decreases with the injection angle and the size of a particle, and increases with the nozzle diameter. However, the powder deposition efficiency $\eta_d \approx b/w$ will decrease as the nozzle diameter increases. If different process parameters are applied to the two powders, the attenuation effect should be treated separately, as Eq. (8) shows.

The width of the part d is set at constant 0.7 mm, the particle radius is assumed to be constant 10 μm. The particle speed v_p, injection angle θ and the nozzle diameter w are set at 10 m/s, 30º and 2 mm respectively. The divergence angle φ is assumed to be 5º, and L is set at 10 mm. The laser beam radius b is 0.6 mm. To determine the attenuated laser power needed to melt the substrate, the FEM simulations on COMSOL Multiphysics® are performed. Since the composition of the part keeps changing during the fabrication, it is difficult to determine the minimum laser power needed for every spot. Therefore, in order to find a minimum P_{att} for every spot, two extreme simulations are run assuming that the substrate consists of only Inconel 718 or Ti-6Al-4V respectively. The power should be able to at least generate a melt pool width large enough to cover the width of the part d. The P_{att} required is then the maximum P_{att} of the two extreme simulations. In the simulation, r_l is fixed to 0.3 mm, and V is fixed to 20 mm/s. A continuous Gaussian beam moves on the symmetrical semi-domain. The energy distribution of the moving Gauss beam under Cartesian coordinate can be expressed as:

$$P_{att}(x,y) = \eta_a P \frac{1}{\sigma\sqrt{2\pi}} e^{-\frac{(x-Vt)^2+y^2}{2\sigma^2}} \tag{12}$$

where σ is the standard deviation which equals to $r_l/3$. The governing heat equation for the temperature evolution of the substrate due to a moving laser heat source is:

$$\rho c_p \frac{\partial T}{\partial t} + \rho c_p \boldsymbol{V} \cdot \nabla T = \nabla \cdot (k \nabla T) \tag{13}$$

where T is the substrate temperature, t is time. The convection and radiation boundary conditions are applied on the peripheral surfaces of the substrate, and the bottom surface is subject to thermal insulation. The minimum P_{att} required for pure Inconel 718 and Ti-6Al-4V are 130 W and 105 W respectively, and we choose the larger one (130 W) as P_{att}.

The remaining process parameter that needs to be predetermined is the powder volumetric feed rate $\dot{V}_p$, and it is related to the manufacturing resolution in the vertical direction, i.e., the height of a single layer h. According to Fig. 2 and from mass conservation,

$$h = \frac{\eta_d \dot{V}_p}{Vd} \tag{14}$$

where the deposition efficiency η_d is assumed to be a constant 0.3 (b/w). Suppose that a 0.3 mm layer height is needed to complete the fabrication in 10 loops. This requires a total volumetric powder feed rate of 14 mm^3/s. For the horizontal direction, we require a 1 mm resolution for the concentration change, which means that the dimension of a cell in the x-axis is 1 mm. The x

position of any cell is represented by the x position of its center. Hence the desired concentrations for a consecutive of cells (i = 1, 2, 3, …, 20) in one layer are $C_{i,des}^{n}$= 2.5%, 7.5%, 12.5%, …, 97.5%.

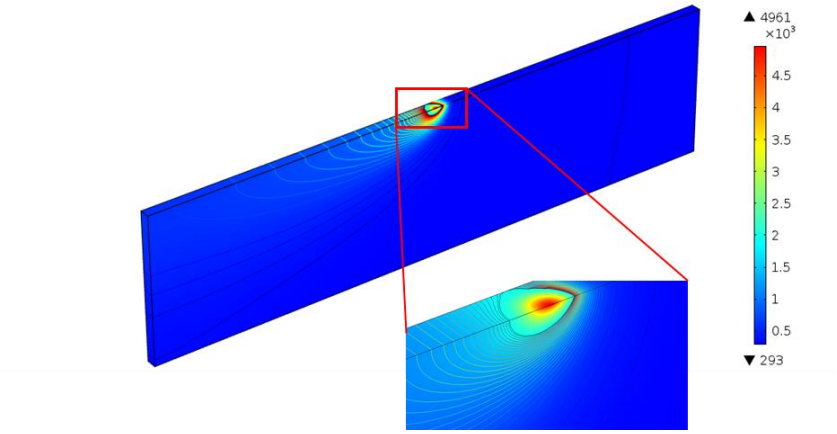

Fig. 6 Typical simulation result (half space due to symmetry) for laser substrate heating. The innermost isotherm line represent the melt pool.

The substrate composition is also critical to the whole process. The best condition is that the substrate has the same composition as the desired FGM part, then the powder concentration will be exactly the same as desired regardless of the dilution effect. However, in most situations the substrate composition is a single material which is most available. Therefore, we start from the substrate which is composed of a single component material only. The first layer or several layers may not achieve the desired concentration but eventually it will. The final part can be fabricated by finally removing the first several sacrificial layers. In this case, we choose Ti-6Al-4V as the substrate material ($C_{i,sub}$ = 1, i = 1, 2, …, 20).

Combining Eqs. (2) - (6) and (9), the locally varied dilution rate and the volumetric powder feed rates ($\dot{V}_p \times C_{i,pow}^{n}$ for Ti-6Al-4V and $\dot{V}_p \times \left(1 - C_{i,pow}^{n}\right)$ for Inconel 718) we should actually apply can be obtained by solving these simultaneous nonlinear equations using Matlab. The calculated locally variation of the two powders' feed rates and the dilution rate for the first layer are shown in Fig. 7. It is understandable that the injected powder at the initial locations is composed of only Inconel 718, since the desired Ti-6Al-4V concentration in the part should be increased gradually from 0 to 1 and the substrate is made of pure Ti-6Al-4V. It can also be imagined that when mixed with the substrate material, several sacrificial layers are needed in order to achieve the desired concentration. These sacrificial layers should finally be cut off via post processing such as lathing or milling. Therefore, a second trial is then conducted to test the achievability of the desired composition. An indicator of the achievability is the maximum/minimum powder feed rate of Inconel 718/Ti-6Al-4V at the initial locations: only when there is no maximum/minimum powder feed rate can we assert that the desired composition is achieved. From Fig. 8 we can see that still the desired composition is not achieved, so the trail is continued. However, contradiction exist that the substrate is made of pure Ti-6Al-4V and that we desire a zero concentration of Ti-6Al-4V in the leftmost location of the part. In this sense, we may assume that the desired composition is achieved whenever the second location does not require a maximum/minimum powder feed rate. Figure 9 shows the powders feed rates and dilution rates when depositing the third layer. We can believe that the desired composition is achieved until this layer, and this "third

layer" will be seen as the actual "first layer". Then, when calculating the remaining layers, their previous layer's physical properties will be calculated directly according to the desired composition.

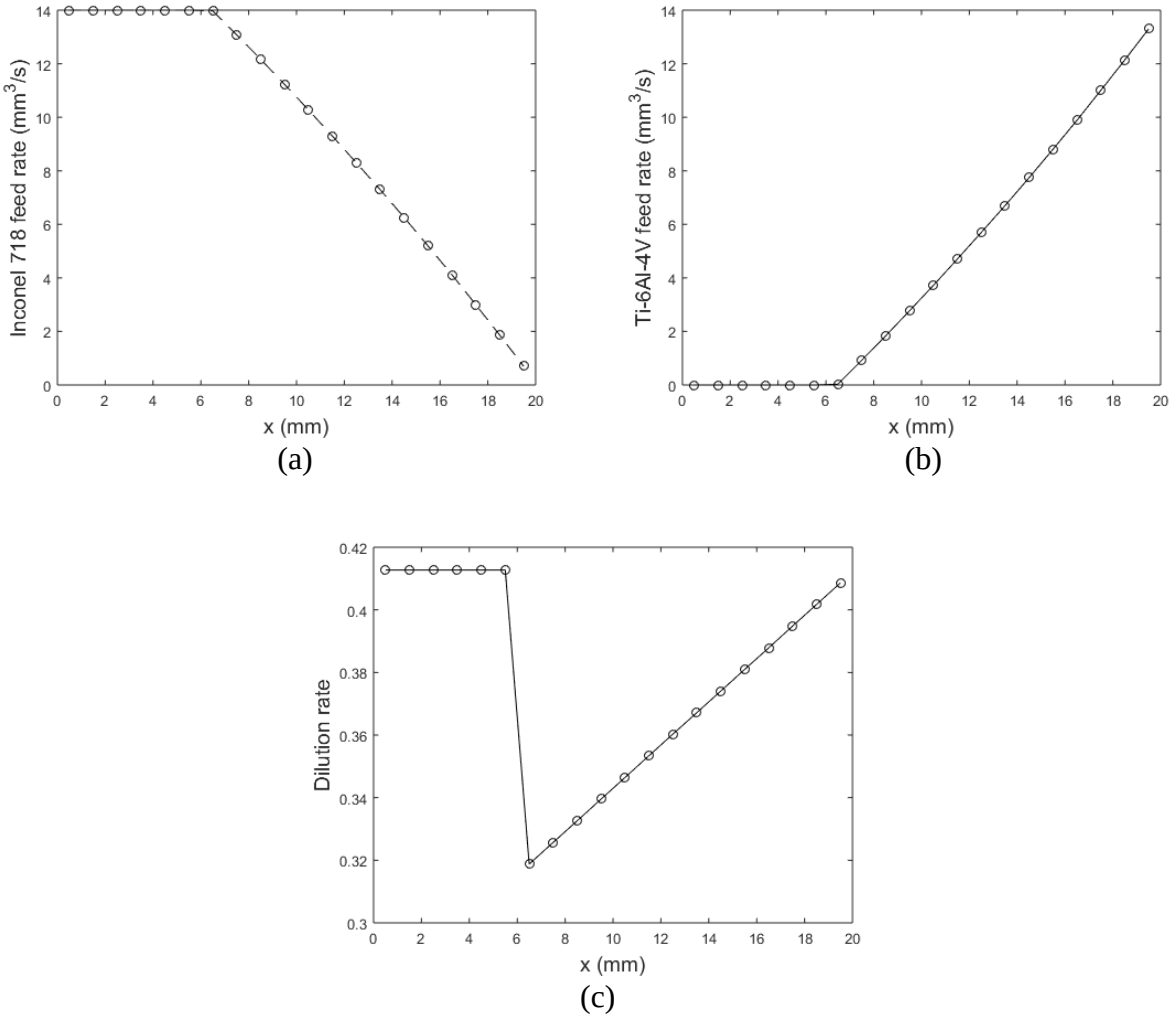

Fig. 7 First trial: (a) the volumetric feed rate of Inconel 718, (b) the volumetric feed rate of Ti-6Al-4V, and (c) the dilution rates at each location.

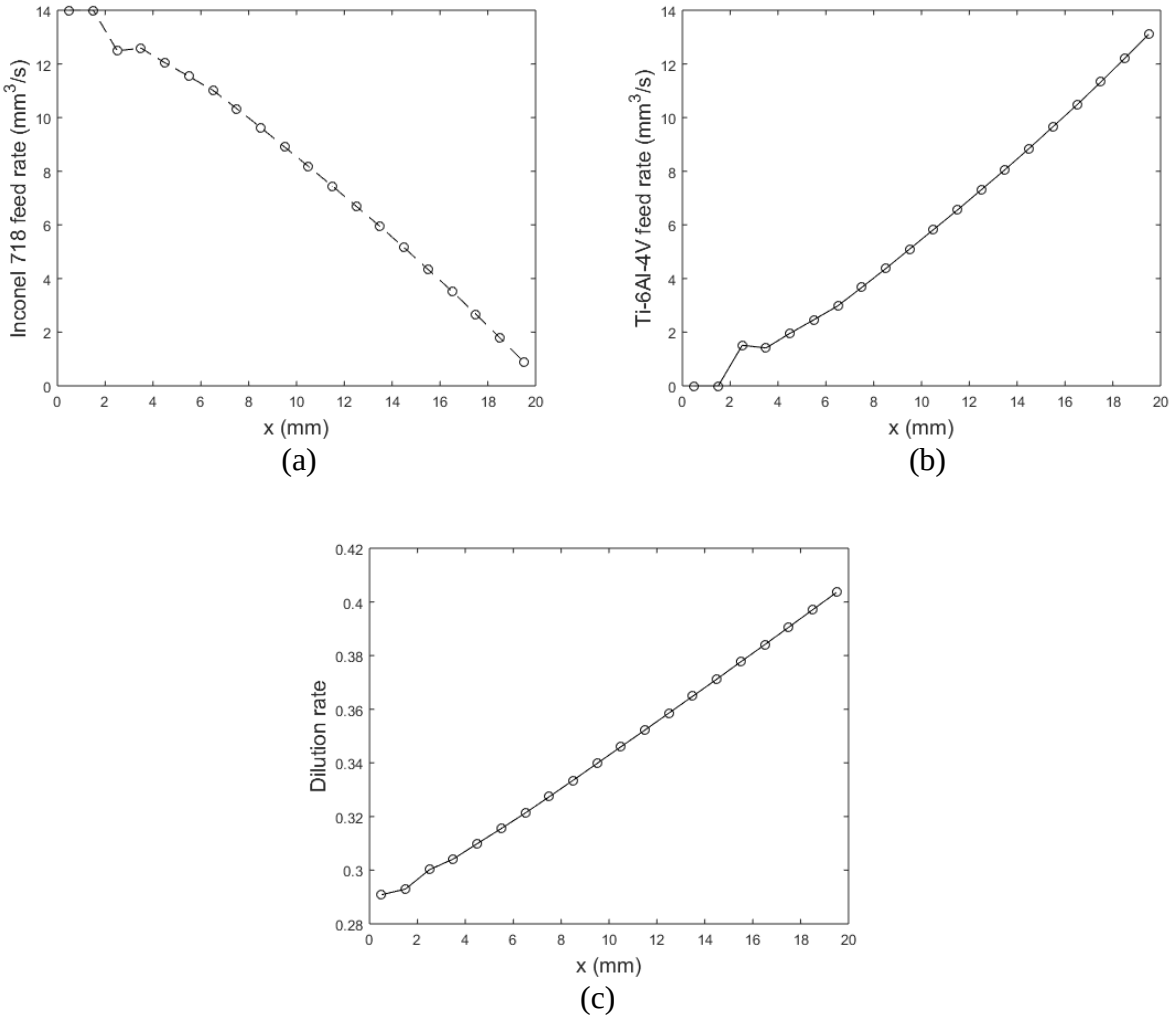

Fig. 8 Second trial: (a) the volumetric feed rate of Inconel 718, (b) the volumetric feed rate of Ti-6Al-4V, and (c) the dilution rates at each location.

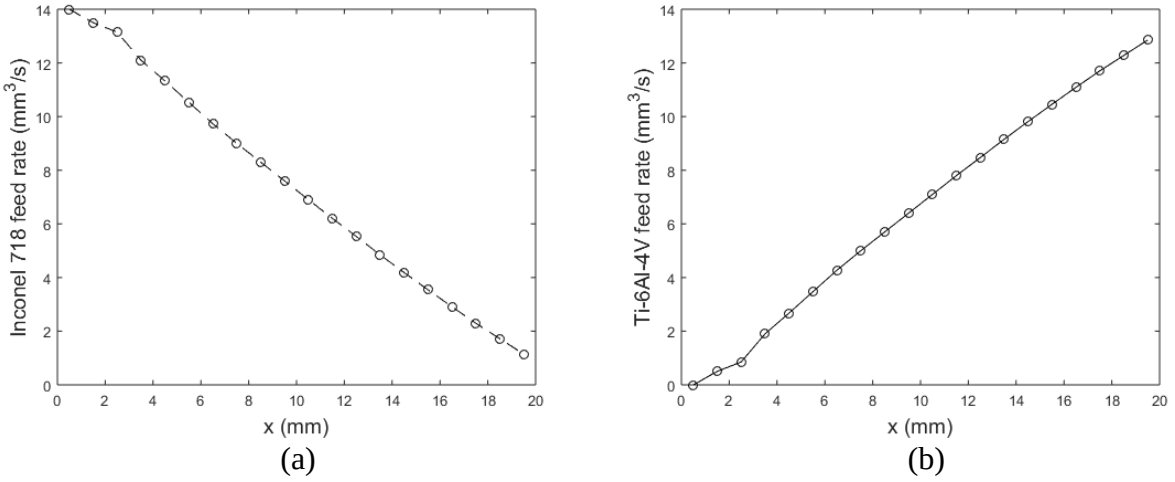

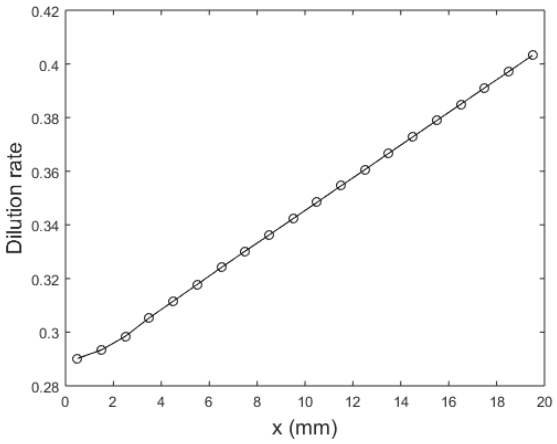

(c)

Fig. 9 Third trial: a) the volumetric feed rate of Inconel 718, (b) the volumetric feed rate of Ti-6Al-4V, and (c) the dilution rates at each location.

Figure 10 shows the plots for the final powders feed rates and the dilution rates at each discrete fabrication location. Since in this case the composition varies in 1D, once the desired composition is achieved and stabilized at the first and second layers, there is no need to vary the powders composition any more among layers. The process becomes a layer by layer iteration after the second layer. It can be seen that the two curves in each of the sub-figures of Fig. 10 are very close. This can be understood and explained by the fact that the more sacrificial layers to cut, the closer the two curves will be. The two curves will eventually be overlapped when the number of sacrificial layers are large enough.

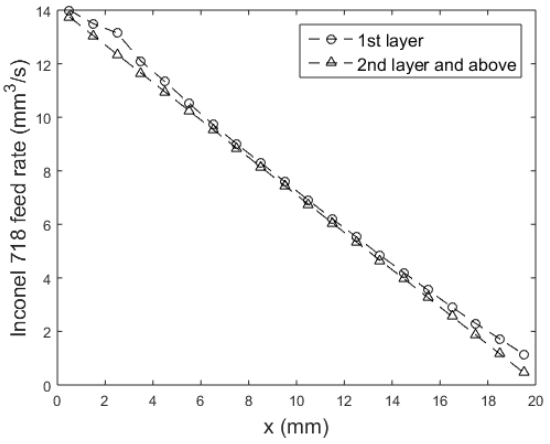

(a)

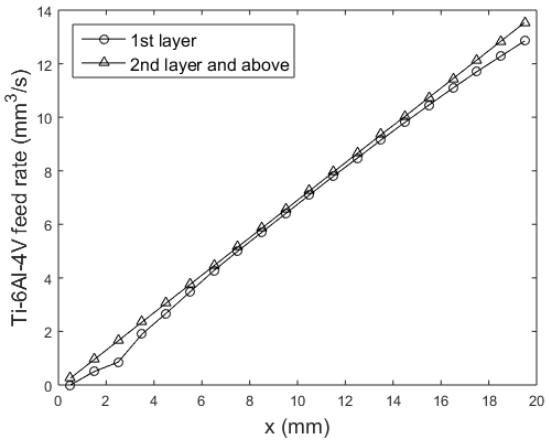

(b)

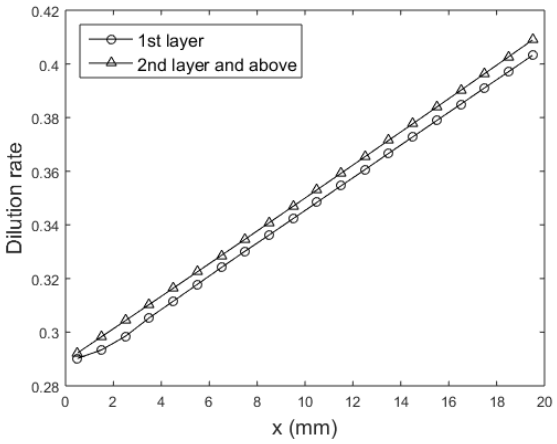

(c)

Fig. 10 Final results: (a) the volumetric feed rate of Inconel 718, (b) the volumetric feed rate of Ti-6Al-4V, and (c) the dilution rates at each location.

An alternative mixture rule is used and the new result (Fig. 11) is compared with the current result (Fig. 10). The equation used for the new mixture rule is expressed in Eq. (10), which is a mass ratio based approach. The trends for the powders feed rates using the two mixture rules are similar with slight difference, while the difference of the dilution rates is apparent. It can be seen that the dilution rate plot for using the mass ratio based mixture rule shows an obvious curved trend, and this causes the differences of the powders feed rates.

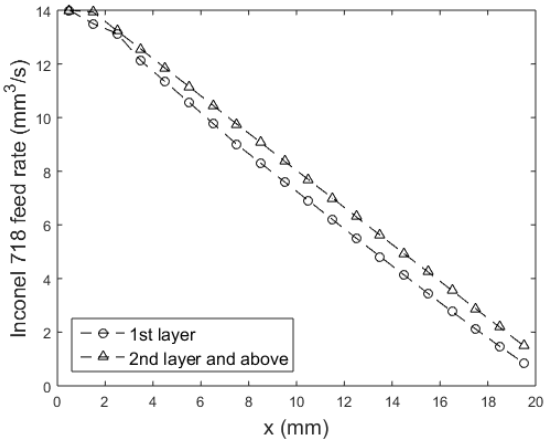

(a)

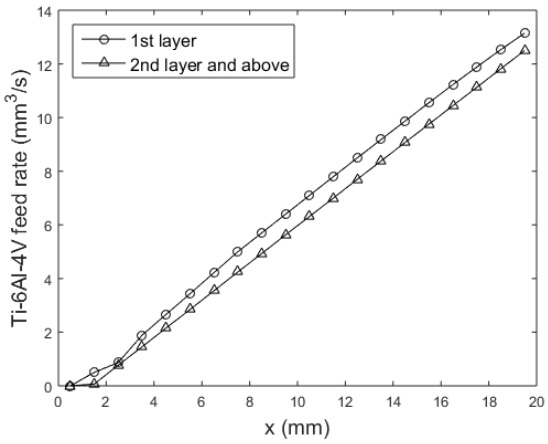

(b)

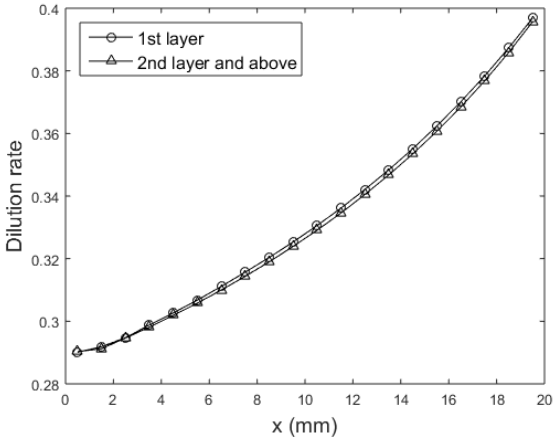

(c)

Fig. 11 Final results using an alternative mixture rule: (a) The volumetric feed rate of Inconel 718, (b) the volumetric feed rate of Ti-6Al-4V, and (c) the dilution rates at each location.

In this case, the total laser power usage is about 25.4%, considering the powder shadowing effect (84.7%) and the laser absorptivity by the substrate (30%). The actual laser power used is calculated as 510.9 W using Eq. (8). The laser power is calculated as a constant value, since the laser attenuation by powder depends on the powders' total volumetric flow rate instead of the concentration of any single powder. Finally, the initial two sacrificial layers (0.6 mm thickness) should be removed.

Case 1 (b):

The alternative building direction of the desired part is illustrated in Fig. 6 (b), where the composition in each layer is constant. For this approach, the concentration in each layer varies from 0 to 1 bottom to up. Inconel 718 is selected as the substrate material ($C_{i,sub}$ = 0, i = 1, 2,…, 10). Apparently, the building direction is not unique: a 1 to 0 manner is completely equivalent, only that the substrate material will be Ti-6Al-4V. Similarly, the Case 1 (a) can be also implemented in a right-to-left manner.

In this case, we assume that all the preset process parameters are the same as Case 1 (a), except the powder volumetric flow rate $\dot{V}_p$. If we still set $\dot{V}_p$ = 14 mm^3/s, resulting in a 0.3 mm layer height, then it will take 66.7 deposition loops (67 layers) to complete the fabrication. In order to make this number an integer and reduce the total number of layers, we set $\dot{V}_p$ = 18.7 mm^3/s to result in a 0.4 mm layer height. The total number of layers then becomes 50. Further reducing the layer number would require an even larger $\dot{V}_p$. Consequently, the deposition efficiency η_d would not simply remain the same, and the dilution rate would be too low to support deposition.

The cell width is fixed to 0.3 mm, and each layer contains 10 cells. Therefore, a 10 × 50 cells array is formulated. The desired concentrations for cells in different layers (n = 1, 2, 3, …, 50) are $C_{i,des}^{n}$= 1%, 3%, 5%, …, 99%. The volumetric feed rates of the two powders and the dilution rate for each layer are shown in Fig. 12. Comparing with Case 1 (a), the results show a linear trend at the beginning of deposition. This is because the concentration gradually changes from 0 (the substrate) to 1, and there is no need to vary the powder concentration in each layer, so that sacrificial layers are not needed. For each layer, the resulted powder concentration is slightly

higher than the desired concentration, since the layer below has a lower concentration. It can be seen from Fig. 12 (c) that the dilution rate is low comparing with Case 1 (a), due to the fact that the $\dot{V}_p$ is larger in this case. The design result for using the alternative mass ratio based mixture rule is similar as the current result (therefore not presented here). The corresponding dilution rate plot is shown in Fig. 12 (d), with a similar curved plot.

Finally, the laser power needed is calculated as 540 W, which is slightly higher than Case 1 (a). In this case, the total laser power usage is 24.1%, considering the powder shadowing effect (80.2%) and the laser absorptivity by the substrate (30%). The reason for the lower laser power usage is also due to the higher total powder volumetric flow rate that results in a stronger shadowing effect.

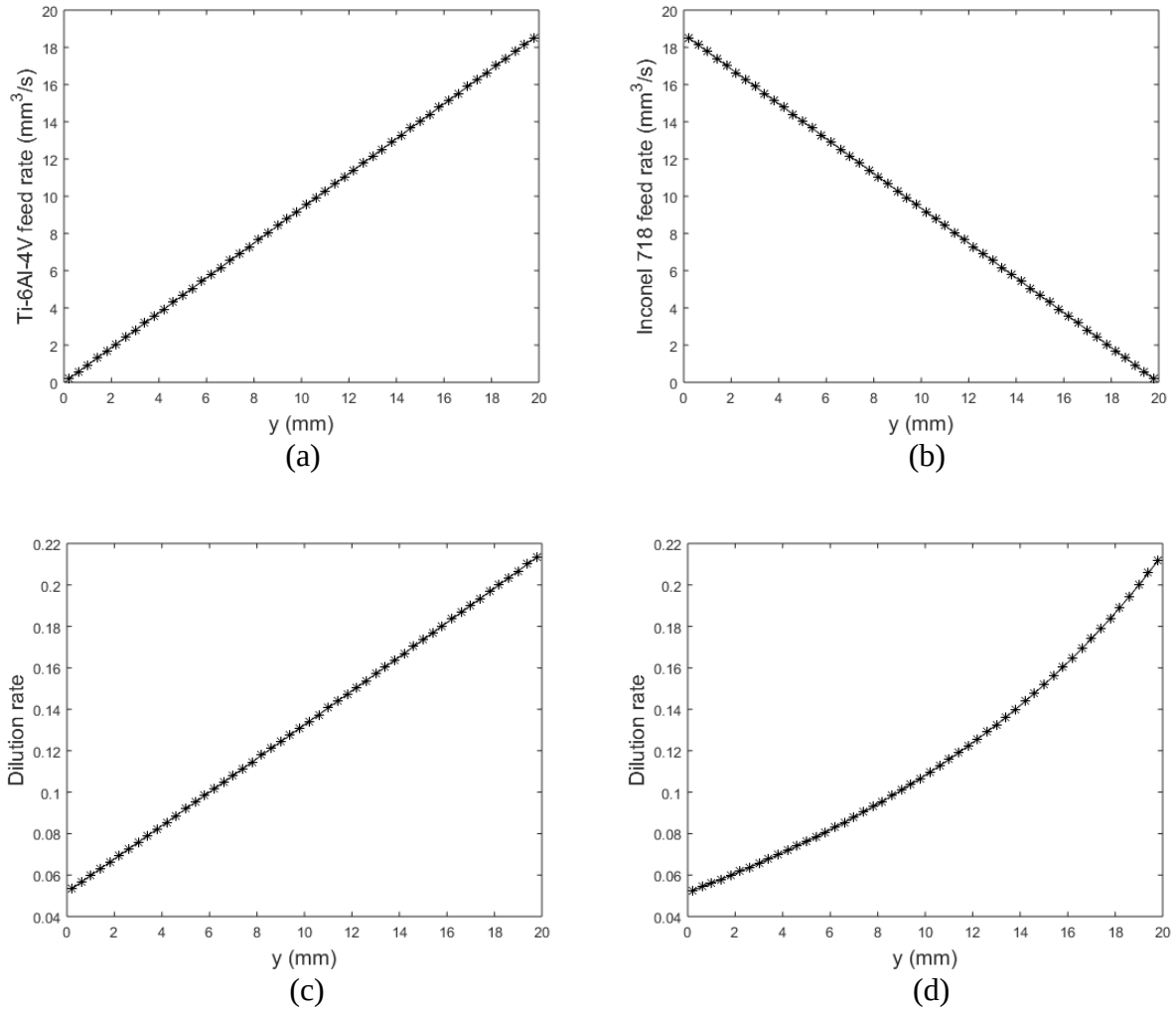

Fig. 12 (a) The volumetric feed rate of Ti-6Al-4V, (b) the volumetric feed rate of Inconel 718, (c) the dilution rate for each layer, and (d) the dilution rate plot using an alternative mixture rule.

Comparing the two fabrication approaches, the first approach varies the powder concentration within a layer and beyond the second layer the variation is repetitive, while the second approach varies the powder concentration among layers but the powder concentration

remains the same within a layer. The dilution rate is a variable within a layer in the former case, while the dilution rate is constant within a layer but varies among layers in the latter case. The main disadvantages of the first approach include: (1) it takes more time for altering the mixing ratio during the fabrication, which lowers the manufacturing precision; (2) it may need a specially made substrate instead of a substrate made of pure material. The main disadvantages of the second approach are: (1) more layers are needed due to the incapability of forming a thick layer, which increases the fabrication time and accumulates deviation/error; (2) the dilution rate is low, which may reduce the connection strength among layers. In summary, the choice of fabrication direction can be different according to different situations.

4.2 Case 2: 2D FGM Part Fabrication

In this case study, process parameters are to be planned to fabricate an FGM part with concentration variation in 2D. The part is of the same dimension as Case 1 (3 mm × 20 mm), and is composed of the same materials (Inconel 718 as material 1 and Ti-6Al-4V as material 2). In order to avoid the zero concentration at end points or edges and thus the appearance of sacrificial layers, the desired concentration is designed to be from 0.2 to 0.8, as shown in Fig. 13 (b). The minimum concentration (C = 0.2) is at the lower left corner, and the maximum concentration (C = 1) is at the upper right corner. The other two corners both have concentrations of 0.5. The transitions among these points are all smooth linear.

The concentration distribution of the desired part follows the function below:

$$C = 0.2 + 0.3 \times \left(\frac{x}{L_x} + \frac{y}{L_y}\right) \tag{15}$$

Consequently, the concentration for Inconel 718 is $0.8 - 0.3 \times \left(\frac{x}{L_x} + \frac{y}{L_y}\right)$. For the 2D case, the concentration varies along both x-axis and y-axis, so there is no significant difference between adopting the two fabrication directions. However, the number of layers are fewer and thus the stability is higher using the horizontal fabrication direction. Therefore, horizontal fabrication is adopted in this study.

Assume that the preset parameters have the same values as Case 1 (a). The P_{att} value is still 130 W, and the actual laser power P can be calculated from Eq. (8). Since the bottom layer of the part has a relatively low concentration of Ti-6Al-4V, Inconel 718 is used as the substrate material in this case.

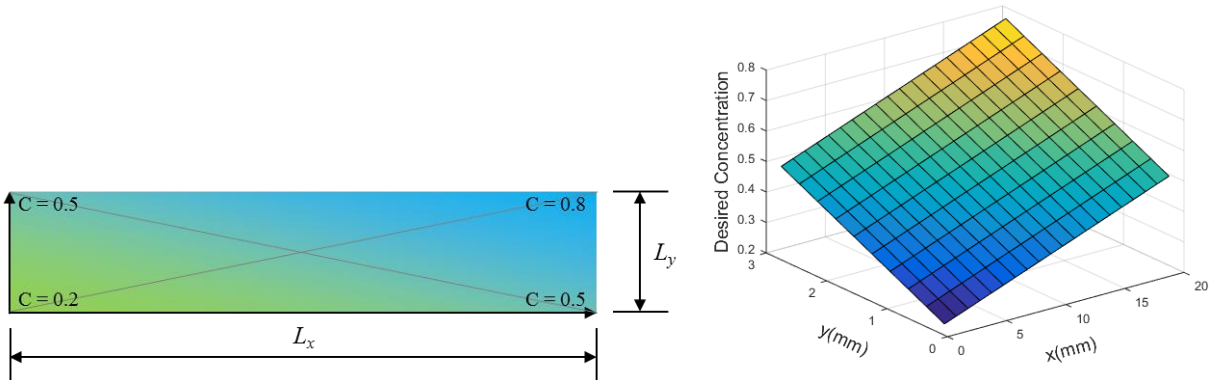

(a) (b)

Fig. 13 Illustration of the desired FGM part with 2D concentration variation.

Following the same calculation procedure, the volumetric flow rates of the two powders and the dilution rates are shown in Fig. 14. It can be seen that except for the first layer, the results for all the other layers are almost parallel with each other. This is understandable since the first layer is built on the substrate, and there is a gap between the substrate concentration and the desired concentration. After the second layer, since the previous layer already achieves the desired concentration, the powder concentration just needs to increase a certain amount to satisfy the gradient concentration variation. Finally, the actual laser power needed is 510.9 W, which is the same as Case 1 (a). In this case, using the alternative mass ratio based mixture rule, the design result is also similar to the current result (not presented). Although it is obvious that Fig. 14 (c) and (d) have detectable differences, their corresponding numbers differ by only around 2.5%. Therefore using the mass ratio based mixture rule generally does not significantly affect the design result. However, as mentioned in earlier text, the results always need to be recalculated whenever a new mixture rule is applied. Although there may be only slightly differences, engineers need to determine the most appropriate mixture rule to use in order to best fit design to applications.

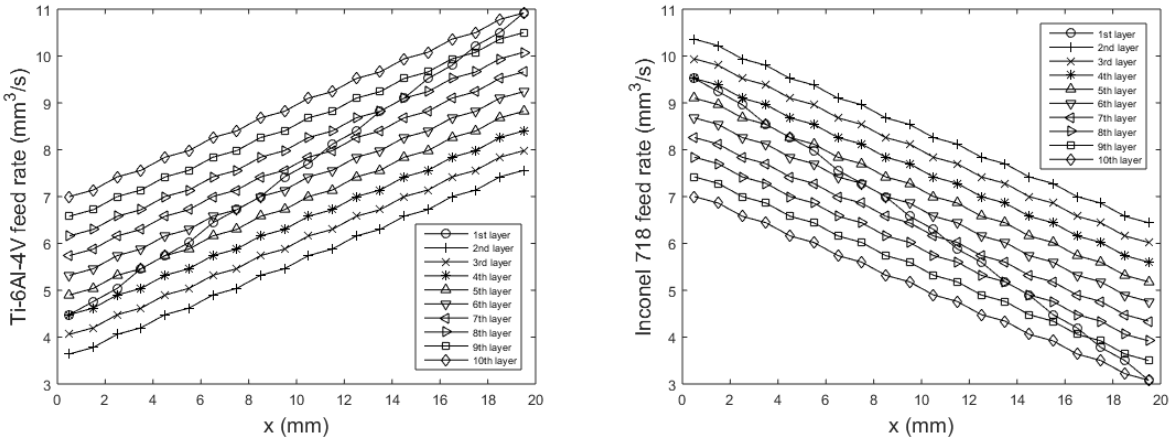

(a) (b)

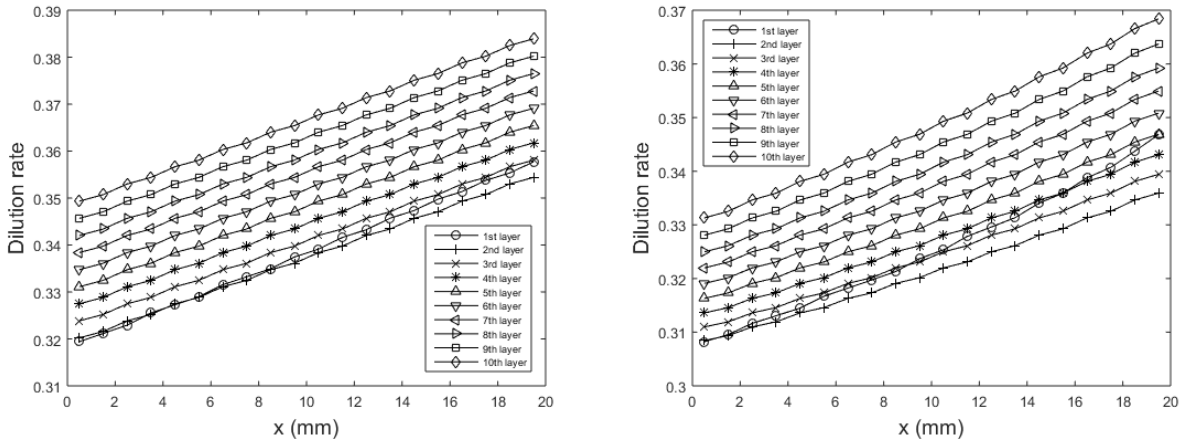

Fig. 14 (a) The volumetric feed rate of Ti-6Al-4V, (b) the volumetric feed rate of Inconel 718, (c) the dilution rates for each location, and (d) the dilution rates plot using an alternative mixture rule.

5 Conclusions and Future Work

This paper proposes a process parameters planning method for the DMD fabrication of FGM part process. Two case studies are presented to demonstrate the method. The varying material properties due to the FGM part composition are considered in the model. The effect of dilution rate on determining the powder concentration needed is also considered to obtain an accurate fabrication. Using the proposed method, the process parameters can be planned prior to the manufacturing process, and the deviation of the material distribution from the desired one can be reduced. This method can serve as an off-line planning process prior to the fabrication. The planned process parameters can be programmed into an executable file readable by the DMD equipment to drive the fabrication.

The two case studies preset most of the parameters, i.e., the attenuated laser power P_{att}, laser scanning speed V, laser spot radius r_l, powder volumetric feed rate $\dot{V}_p$, injection angle θ_i, nozzle diameter w, particle speed v_{pi}, particle radius r_{pi}, powder divergence angle φ, the distance between the nozzle center and the spot center L, and the width of the thin-walled part d. These parameters are related with the determination of the powder concentration and the laser power, and they are not necessarily as what we set in this paper. For example, if setting the laser scanning speed to a lower value, the substrate is easier to be melted. Consequently, the dilution rate might end up higher, and/or the attenuated laser power might end up lower, in which case the powder concentration and laser power should be recalculated. Actually, these preset parameters can be played with and adjusted according to equipment settings and different requirements. For example, to increase the fabrication resolution, we may reduce the powder size and the laser beam dimension.

For better application of the proposed method, future work may include: (1) considering more complicated FGM part concentration variation, including the 3D cases; (2) investigating the effects of the variation of different preset parameters on the final decision to help better understand the process; (3) taking into account the material properties variation due to the temperature change during fabrication; (4) involving more physical based models and/or simulations, such as the particle-laden turbulent feed gas flow model; and (5) manufacturing parts using DMD and

conducting electron microscope imaging and/or mechanical property test experiments to validate the results.

References

[1] Kumar, V., and Dutta, D., 1997, "An Approach to Modeling Multi-Material Objects," presented a Third Symposium on Solid Modeling and Applications, Atlanta, GA, 1997.

[2] Huang, J., 2000, "Heterogeneous Component Modeling and Optimal Design for Manufacturing," *Ph. D. thesis*, Clemson University, 2000.

[3] Schwendner, K. I., Banerjee, R., Collins, P. C., Brice, C. A., and Fraser, H. L., 2001, "Direct Laser Deposition of Alloys from Elemental Powder Blends," *Scripta Materialia*, Vol. **45**(10), pp. 1123-1129.

[4] Collins, P.C., Banerjee, R., and Fraser, H.L., 2003, "The Influence of the Enthalpy of Mixing During the Laser Deposition of Complex Titanium Alloys Using Elemental Blends," *Scripta Materialia*, Vol. **48**(10), pp. 1445-1450.

[5] Domack, M.S., and Baughman, J.M., 2005, "Development of Nickel-Titanium Graded Composition Components," *Rapid Prototyping Journal*, Vol. **11**(1), pp. 41-51.

[6] Zhong, M., Liu, W., Zhang, Y., and Zhu, X., 2006, "Formation of WC/Ni Hard Alloy Coating by Laser Cladding of W/C/Ni Pure Element Powder Blend," *International Journal of Refractory Metals and Hard Materials*, Vol. **24**(6), pp. 453-460.

[7] Yue, T. M., and Li, T., 2008, "Laser Cladding of Ni/Cu/Al functionally graded coating on magnesium substrate," *Surface and Coatings Technology*, Vol. **202**(23), pp. 3043-3049.

[8] Hofmann, D.C., Roberts, S., Otis, R., Kolodziejska, J., Dillon, R.P., Suh, J., Shapiro, A.A., Liu, Z., and Borgonia, J., 2014, "Developing Gradient Metal Alloys through Radial Deposition Additive Manufacturing," *Nature Scientific Reports*, July 19.

[9] Lewis, G. K., and Schlienger, E., 2000, "Practical Considerations and Capabilities for Laser Assisted Direct Metal Deposition," *Materials and Design*, Vol. **21**(4), pp. 417-423.

[10] Liu, W., and DuPont, J.N., 2003, "Fabrication of Functionally Graded TiC/Ti Composites by Laser Engineered Net Shaping," *Scripta Materialia*, Vol. **48**(9), pp. 1337-1342.

[11] Pintsuk, G., Brünings, S.E., Döring, J.-E., Linke, J., Smid, I., and Xue, L., 2003, "Development of W/Cu – functionally graded materials," Fusion Engineering and Design, Vol. **66-68**, pp. 237-240.

[12] Yakovlev, A., Trunova, E., Grevey, D., Pilloz, M., and Smurov, I., 2005, "Laser-Assisted Direct Manufacturing of Functionally Graded 3D Objects," *Surface and Coatings Technology*, Vol. **190**(1), pp. 15-24.

[13] Qi, H., and Mazumder, J., 2006, "Laser Cladding Based Solid Freeform Fabrication and Direct Metal Deposition," *Proceedings of the MSEC*, pp. 87-100.

[14] Ocylok, S., Weisheit, A., and Kelbassa, I., 2010, "Functionally Graded Multi-Layers by Laser Cladding for Increased Wear and Corrosion Protection," *Physics Procedia*, Vol. **5**, pp. 359-367.

[15] Soodi, M., and Masood, S.H., 2014, "Tensile Strength of Functionally Graded and Wafer Layered Structures Produced by Direct Metal Deposition," *Rapid Prototyping Journal*, Vol. **20**(5), pp. 360-368.

[16] Shah, K., Haq, I., Khan, A., Shah, S.A., Khan, M., and Pinkerton, A.J., 2014, "Parametric Study of Development of Inconel-Steel Functionally Graded Materials by Laser Direct Metal Deposition," *Materials & Design*, Vol. **54**, pp. 531-538.

[17] Griffith, M.L., Harwell, L.D., Romero, J.A., Schlienger, E., Atwood, C.L., and Smugeresky, J.E., 1997, "Multi-material processing by LENS™," *Proceedings of the Solid Freeform Fabrication Symposium*, Austin, TX.
[18] Huang, J., and Fadel, G.M., 2000, "Heterogeneous Flywheel Modeling and Optimization", *Journal of Materials and Design*, Vol. **21**(2), pp.111-125.
[19] Morvan, S., Fadel, G.M., Keicher, D., and Love, J., 2001, "Manufacturing of a Heterogeneous Flywheel on a LENS Apparatus," Proceedings of Symposium on Solid Freeform Fabrication, University of Texas at Austin, Austin, Texas, August 2014.
[20] Morvan, S., 2001, "MMa-Rep, a Representation for Multimaterial Solids," *Ph. D. thesis*, Clemson University.
[21] Huang, J., and Fadel, G.M., 2001, "Bi-Objective Optimization Design of Heterogeneous Injection Mold Cooling Systems", *Journal of Mechanical Design*, Vol. **123**(2). pp. 225-239.
[22] Chapter 6: Multi-Material Representation and Design Issues – in Software Solutions for Rapid Prototyping, MCB Press, Ian Gibson, Editor, pp. 155-224, 2002.
[23] Huang, J., Fadel, G.M., Blouin, V., and Grujicic, M., 2002, "Bi-objective Optimization Design of Functionally Gradient Materials", *Journal of materials, design and applications*, Vol. **23**(7), pp. 657-666.
[24] Shin, K., Natu, H., Dutta, D., and Mazumder, J., 2003, "A Method for the Design and Fabrication of Heterogeneous Objects," *Materials and Design*, Vol. **24**(5), pp. 339-353.
[25] Thivillon, L., Bertrand, P., Laget, B., and Smurov, I., 2009, "Potential of Direct Metal Deposition Technology for Manufacturing Thick Functionally Graded Coatings and Parts for Reactors Components," *Journal of Nuclear Materials*, Vol. **385**(2), pp. 236-241.
[26] Muller, P., Mognol, P., and Hascoet, J., 2013, "Modeling and Control of a Direct Laser Powder Deposition Process for Functionally Graded Materials (FGM) Parts Manufacturing," *Journal of Materials Processing Technology*, Vol. **213**(5), pp. 685-692.
[27] Yan, J., Battiato, I., and Fadel, G.M., 2014, "Optimization of Multi-Materials In-Flight Melting in Laser Engineered Net Shaping (LENS) Process," Proceedings of Symposium on Solid Freeform Fabrication, University of Texas at Austin, Austin, Texas, August 2014.
[28] Yan, J., Masoudi, N., Battiato, I., and Fadel, G., 2015, "Optimization of Process Parameters in Laser Engineered Net Shaping (LENS) Deposition of Multi-Materials," Proceedings of the ASME 2015 International Design Engineering technical Conferences & Computers and Information in Engineering Conference (IDETC/CIE), Boston, Massachusetts, August 2015.
[29] DebRoy, T., and David, S.A., 1995, "Physical Processes in Fusion Welding," *Reviews of Modern Physics*, Vol. **67**(1), pp. 85-112.
[30] Yang, Z., 2000, "Modeling Weldment Macro and Microstructure from Fundamentals of Transport Phenomena and Phase Transformation Theory," Ph.D. thesis, Pennsylvania State University.
[31] He, X., Fuerschbach, P.W., and DebRoy, T., 2003, "Heat Transfer and Fluid Flow during Laser Spot Welding of 304 Stainless Steel," *Journal of Physics D: Applied Physics*, Vol. **36**(12), pp. 1388-1398.
[32] Picasso, M., and Hoadley, A.F.A., 1994, "Finite Element Simulation of Laser Surface Treatments Including Convection in the Melt Pool," *International Journal of Numerical Methods for Heat & Fluid Flow*, Vol. **4**(1), pp. 61-83.
[33] Ki, H., Mohanty, P.S., and Mazumder, J., 2002, "Modeling of Laser Keyhole Welding: Part II. Simulation of Keyhole Evolution, Velocity, Temperature Profile, and Experimental Verification," *Metallurgical and Materials Transactions, A*, Vol. **33A**(6), pp. 1831-1842.

[34] Morville, S., Carin, M., Peyre, P., Gharbi, M., Carron, D., Masson, P. L., and Fabbro, R., 2012, "2D Longitudinal Modeling of Heat Transfer and Fluid Flow during Multilayered DLMD Process," *Journal of Laser Applications*, Vol. **24**(3), pp. 032008(1-9).
[35] Unocic, R.R., and DuPont, J.N., 2003, "Composition Control in the Direct Laser-Deposition Process," Metallurgical and Materials Transactions B, Vol. **34B**(4), pp. 439-445.
[36] Wells, A.A., 1952, "Heat Flow in Welding," *Welding Journal*, Vol. **315**(5), pp. 263s-267s.
[37] DuPont, J.N., and Marder, A.R., 1995, "Thermal Efficiency of Arc Welding Processes," *Welding Journal*, Vol. **74**, pp. 406s-416s.
[38] Jouvard, J.M., Grevey, D.F., Lemoine, F., and Vannes, A.B., 1997, "Continuous Wave Nd: YAG Laser Cladding Modeling: a Physical Study of Track Creation during Lower Power Processing," *Journal of Laser Applications*, Vol. **9**(1), pp. 43-50.
[39] Lin, J., 2000, "Laser Attenuation of the Focused Powder Streams in Coaxial Laser Cladding," *Journal of Laser Applications*, Vol. **12**(1), pp. 28-33.
[40] Han, L., Liou, F.W., and Phatak, K.M., 2004, "Modeling of Laser Cladding with Powder Injection," *Metallurgical and Materials Transactions B*, Vol. **35**(6), pp. 1139-1150.
[41] Pinkerton, A. J., 2007, "An Analytical Model of Beam Attenuation and Powder Heating during Coaxial Laser Direct Metal Deposition," *Journal of Physics D: Applied Physics*, Vol. **40**(23), pp. 7323-7334.
[42] Zhou, J., and Liu, H., 2009, "Laser Rapid Manufacturing Technology and Application," Beijing: Chemical Industry Press.
[43] Tabernero, I., Lamikiz, A., Martínez, S., Ukar, E., and Lacalle, L. N., 2012, "Modeling of Energy Attenuation due to Powder Flow – Laser Beam Interaction during Laser Cladding Process," *Journal of Materials Processing Technology*, Vol. **212**(2), pp. 516-522.
[44] Pottlacher, G., Hosaeus, H., Kaschnitz, E., and Seifter, A., 2002, "Thermophysical Properties of Solid and Liquid Inconel 718 Alloy," *Scandinavian Journal of Metallurgy*, Vol. **31**(3), pp. 161-168.
[45] Boivineau, M., Cagran, C., Doytier, D., Eyraud, V., Nadal, M.H., Wilthan, B., and Pottlacher, G., 2006, "Thermophysical Properties of Solid and Liquid Ti-6Al-4V (TA6V) Alloy," *International Journal of Thermophysics*, Vol. **27**(2), pp. 507-529.
[46] Chen, H., Pinkerton, A.J., and Li, L., 2011, "Fibre Laser Welding of Dissimilar Alloys of Ti-6Al-4V and Inconel 718 for Aerospace Applications," *International Journal of Advanced Manufacturing Technology*, Vol. **52**(9), pp. 977-987.